Hindawi
International Journal of Energy Research
Volume 2024, Article ID 6209170, 14 pages
https://doi.org/10.1155/2024/6209170

WILEY | Hindawi

Research Article

Saving Energy and High-Efficient Inspection to Offshore Wind Farm by the Comprehensive-Assisted Drone

Xianfei Huang[1] **and Gaocai Wang**[2]

[1]*School of Electrical Engineering, Guangxi University, Nanning 530004, China*
[2]*School of Computer and Electronic Information, Guangxi University, Nanning 530004, China*

Correspondence should be addressed to Gaocai Wang; gcwang@gxu.edu.cn

Received 1 September 2023; Revised 2 January 2024; Accepted 25 January 2024; Published 8 February 2024

Academic Editor: Ayman Al-Quraan

Facing the method's limitations of the existing drone inspection on offshore wind farms, we adopt a new comprehensive-assisted drone automated inspection scheme under the comprehensive assistance. Our objectives are saving energy and high-efficient inspection. The such inspection is used to formulating the two mixed-integer nonlinear programming problems based on two new drone basic models: the mobile edge computing driven drone computation system model and the drone flight model. To solve the problems, we split them into four subproblems, and a new improved heuristic algorithm is created to address. In turns, the waypoints, total inspection time, inspection energy consumption, and traveling distance of unmanned aircraft vehicle (UAV) and the traveling distance of boat are obtained by K-means algorithm and the smallest enclosing circle (SEC) algorithm, the Lin-Kernighan Heuristic 3 (LKH-3) algorithm, and the LKH. Finally, conducting the comprehensive optimization and simulation, the simulation numeric results are gotten. The simulation results demonstrate that as for the two aspects of the total energy consumption and inspection efficiency under different data amount and average wind speed, the scheme improves at most 44% and 23.5% than the current other three; the scheme achieves the objective of saving energy and high-efficient inspection.

1. Introduction

Recent decade, clean energy has been paid a great attention. In particular, wind power will grow greatly in the next five years [1]. This high increase will inevitably rely on more large-scale application of wind turbines, further developing to deep sea, forming the large amount of various large-scale wind farms. So, the wind turbine failure also increases with their more widely applications. The wind turbines especially in the offshore wind farm [2] required more checking to ensure the safe and continuous operation, because they usually operate in a harsher environment and have relatively higher failure rates [3]. The failures usually and mainly occur on the blades [4]. However, the traditional sensors can hardly directly and sensitively reflect the microdamage on the blade surface [5, 6]. But, a High Definition camera sensor (HDCS) combined with image recognition technology can reflect the situation [5, 6]. However, the HDCS and the traditional sensors are hard usefully to install and maintain on the wind turbine offshore [1], thanks for the unmanned aircraft vehicle (UAV) equipped with HDCS possessing mobility and adjustable flight altitudes [7]. This provides conveniently to detect the wind turbine blades and offers a visualization service in many promising application scenarios [8], including blade damage inspection in the wind turbine [5, 9–11]. This provides the solid basis on saving energy and high-efficient inspection to offshore wind farm.

To improve the inspection efficiency of the whole wind farm, utilizing UAV equipped with HDCS, scientists or researchers have proceeded some far and wide study on the following various aspects: the deployment and flight trajectory of the UAV [1, 12–14], the routing of inspecting the wind turbine [1, 6], the wind speed [1, 12–17], the traveling salesman problem (TSP) [1, 12], the wireless communication environment [12], and the cost including the location

selecting and building of the automated airports [1]; moreover, the vehicle-assisted UAV [13] or mobile edge computing (MEC) server [12, 18, 19], the local computing [18–20] and data offloading [20], and the advancement of massive machine-type connectivity (mMTC) and satellite technologies [21] have made a great progress. But for the future developing great amount of large-scale offshore wind farms that is facing more wide and deep sea, there are still limitations of some scheme for the inspection schemes:

(i) Not enough consideration of the UAV total inspection energy consumption problem [1, 6, 12, 13]

(ii) The scalability and flexibility of which a fixed automated airport lacks [1, 12]; the UAV charging station problem [21]

(iii) Nonconsideration of the UAV computation capability and the wind condition problem [6, 13]

1.1. Motivation and Contributions. We are enlightened by the methods of inspection land wind farms [12, 13] and motivated by the schemes of inspection offshore wind farms [1, 21]. A new comprehensive-assisted UAV automation inspection scheme of the future offshore wind farm, for collecting the health data of offshore wind turbine mainly including blades, is proposed and used. That is, under MEC server assistance, exploiting a boat-assisted UAV scheme deploys UAVs to detect wind turbine and process sensory data in wind farms [12]. Drone is equipped with HDCS, communication modules, and computation units [1, 12], further comprehensively considering the saving energy, high-efficient, and optimal route planning. At present, this type of comprehensive research on inspecting offshore wind farms is yet seldom.

The comprehensive scheme is aimed at exploiting the following current advance technologies: (1) the integration strengths of the low earth orbit (LEO) satellite and the massive machine-type connectivity (mMTC, i.e., LoRaWAN), which is specially used in remote areas [12, 21] (or remote marine areas), (2) the MEC technological advantages [12, 20], and (3) the scalability and flexibility of the movement battery station or automated airport (use of truck onshore [22] or boat offshore [6]). As for the UAV of the scheme, it is assisted by the LEO satellite and the mMTC (i.e., LoRaWAN), in which, there are two ways (indirect LoRaWAN and direct LoRaWAN) [21]; it can be based on the practical situation to choose. Based on the real conditions, the massive machines for connectivity can be load on the boat. The boat possesses an extra battery and charging equipment as a station (BBS) and a control center. The center is equipped with the equipment similar to the ground stations (GSs) [12], combining with LEO satellite and MEC servers together, constructing a new space-air-boat integrated network (SABIN), similar to the space-air-ground integrated network (SAGIN) architecture [12]. So, seamless and flexible network coverage for wind farms is provided.

For the problems of the saving energy and high-efficient inspection, the scheme objectives are to minimize the total energy consumption of the detection and optimize the inspection efficiency via the optimal route planning and then the optimal inspection time. The two problems (i.e., the two aims) are modeled as two combinatorial optimization problems based on the UAV and BBS routing planning. These are the mixed-integer nonlinear programming problem (MINLP). We address them by solving the following four optimization subproblems: the UAV detection energy consumption of each wind turbine, the power consumption of the UAV under the wind condition, and the route planning of the UAV and the BBS, respectively. For the four subproblems, an improved heuristic algorithm (i.e., mixed optimization algorithm (MOA)), which combined the Lin-Kernighan Heuristic 3 (LKH-3), smallest enclosing circle (SEC) algorithm, and K-means clustering algorithm, is developed in this paper, to solve the combinatorial optimization problems. This paper contributes as follows:

(i) The new comprehensive MEC and BBS-assisted UAV automating inspection scheme for offshore wind farms is proposed, which makes drone inspection with scalability and flexibility

(ii) Two new basic models are employed in the scheme for research. One is a new MEC-driven UAV computation model, and another is a new UAV power consumption model under wind conditions. It makes the inspection trending to the real scene

(iii) To solve the combinatorial optimization problems, we have developed an improved heuristic algorithm consisted of three different type algorithms of LKH-3, SEC, and K-means

(iv) The total energy consumption of the inspection has been minimized, and the efficiency of inspecting wind farms has been optimized. The scheme performs the best

(v) The optimal routes of the BBS and the UAV are obtained via the improved heuristic algorithm

1.2. Relative Research Work and Their Experiences. For the wind turbine, some researchers focus on using the advanced sensor to detect the health of wind turbine blades. Zhao et al. [23] successfully extracted blade parameters and detected blade fault by the Doppler radar sensor based on the time-Doppler features of the horizontal axis wind turbine (HAWT). Avendaño-Valencia et al. [24] predicted the short-term fatigue damage equivalent loads (DEL) on the wind turbine blade via the deployment wind field inflow sensors and/or load sensors. Xu et al. successfully developed a waveform-based feature extraction method and used it to obtain the original acoustic emission (AE) signals by AE sensor array arrangement to monitor the blade health [25]. However, the various traditional sensors above are hard, direct, and sensitive to reflect the microdamage on the blade surface [5, 6]. Aiming the challenge of reflecting the microdamage, some researchers used the UAV with an HD camera sensor and image recognition to detect the blade [1, 5, 6, 9–11]. For example, Yang et al. [5] used the Otsu method to recognize the damaged image taken by UAV HD camera,

and this method had an excellent performance. Huang et al. [6] reported that the UAV with HD camera under the boat assistance detects the blade microdamages of wind turbines for the modern large-scale offshore wind farm in details. Wang and Zhang [9] applied the Haar-like feature to depict crack regions and trained a cascading classifier for detecting cracks. It made the crack recognition in images taken by UAV HD camera faster. In the meantime, a parallel sliding window method was developed by Wang et al. [10] to scan those wind turbine blade surface cracks via analyzing blade images captured by UAV HD camera and successfully deployed on devices of UAVs. Xu et al. employed the alternating direction method of multiplication to reduce the hardware device requirements for image recognition and improve the performance of the image recognition device on UAV [11]. The above research works improved the blade failure detection efficiency and precision in one single wind turbine, but did not still extend, and apply in the inspection efficiency that is facing more large-scale offshore wind farms in the future.

In order to improve the inspection efficiency of the whole wind farm, researchers have proceeded many greatly effective studies.

Chung et al., Cao et al., and Baik and Valenzuela have presented that the deployment and flight trajectory of the UAV impact the efficiency of inspecting wind farms [1, 12, 13]. They suggested that the wind speed is an indispensable condition in the inspection [1, 12]. Although the wind speed changes from time to time [15], either on the sea or on land, in most cases, the wind speed is assumed to be a constant in creating a flight path. For examples, Chung et al. [1] reported the routing of inspecting the wind turbine and considered the influence of average wind speed on the inspection. Luo et al. [16] showed that under steady wind speed, a UAV path planning solution is feasible. Thibbotuwawa et al. [14] used constant wind speed in creating flight plans (including flight paths). Coombes et al. considered that steady uniform wind speed for a flight path of the UAV aerial survey is realistic [17]. Wind speed makes an impact on the UAV inspection efficiency and its total inspection energy consumption. Chung et al. [1] considered not only the influence of the wind speed on the inspection efficiency of the offshore wind farm but also used the TSP to improve the UAV inspection efficiency but had not considered the influence of the wind condition on the wireless communication environment and the total energy consumption of the UAV inspection wind farm. Meanwhile, establishing and maintaining the fixed automated airport offshore is still very hard. If many stationary automated airports are built offshore, the cost of establishment and maintenance will be very high. In addition, manual maintenance for each offshore airport results in an increase in the risk and labor cost for the maintenance worker. Cao et al. [12] improved the efficiency of inspecting wind farms by UAV using the TSP by considering the impact of the wireless communication environment and wind speed on the wind farm. But the as-used ground control center station is fixed, and the application scenario was on land. Baik and Valenzuela [13] reduced the total operation time for inspecting a wind farm, and this UAV inspection is assisted by a ground vehicle with extra batteries and charging equipment available. However, as an automated inspection scheme, the total energy consumption of the UAV inspection wind farm, the UAV computation capability, and the wind condition are not considered. Leveraging the advancement of massive machine-type connectivity (mMTC) and satellite technologies, Ullah et al. [21] investigated the potential of these to enable remote monitoring of the offshore wind farms. Finally, they used realistic deployment and traffic and advanced propagation and collision models, proving the indirect architecture and direct approach feasibility and packet delivery probability numerically when implemented over mMTC (i.e., LoRaWAN) technology. However, a part of collecting wind turbine blade data techniques in [21] scheme was relied on the techniques of [12]. Especially, when a battery capacity-limited UAV needs to charge, for the wider and far marine large-scale wind farms, the reliability of a fixed onshore charging station should be worthy to be cautiously considered. Huang et al. [6] had made some progresses at two aspects and overcome the following limitations: one is the existing methods lack scalability and flexibility due to the UAV requirements for battery exchange stations; another is the "record-offload-process" further limits the application of conventional UAVs for wind farm inspections. But there are some unsatisfactory considerations of the effects from the wind speed and the exploiting of modern technological advantages.

Therefore, some issues in inspecting the entire offshore wind farms by UAV are still wide open: not enough consideration of the total inspection energy consumption problem [1, 6, 12, 13], the lack of a moving automated airport scalability and flexibility [1, 12], the UAV charging station problem [21], and nonconsideration of the UAV computation capability and the wind condition problem [6, 13].

More importantly, the experience about leveraging the MEC server [12, 18, 19] and the local computing [18–20] and data offloading [20] provides us an important reference. Cao et al. reported that the MEC server can improve the inspection efficiency and computation capability of UAVs in land wind farms [12]. Sun et al. [20]. combined local computing and data offloading into a joint computation algorithm for proposing a new optimal scheme, which has an excellent performance. They also reported that data offloading becomes preferable when this data size grows more and more. A unified system design that includes MEC and wireless power transfer (WPT) is proposed by Wang et al. [18]. The system could charge power for the user's local computation and made itself obtaining excellent system performance by offloading data to the MEC server. Zhang et al. investigated the partial computation offloading mode in a MEC system on the UAV, and the system obtained the maximum computation efficiency [19]. In a word, using MEC technology can improve UAV computation capability. Therefore, the MEC system can be employed to improve the inspection performance of offshore wind farms.

Besides, notably, the LKH algorithm demonstrated strong optimization capabilities [26]. The researchers highlighted the importance of the LKH algorithm for addressing

a distance-constrained capacitated vehicle routing problem (DCVRP), which is a special case of the TSP; the DCVRP is known to be a strongly NP-hard problem [27], and deriving a precise analytical mathematical solution is highly challenging. However, the LKH-3 algorithm has been proved by Helsgaun [28] to be a well-suited heuristic algorithm for effectively tackling such strongly NP-hard problems.

In summary, using the strengths of the technologies above, i.e., the LEO satellite and LoRaWAN, the UAV with an HD camera sensor and image recognition, the MEC technology, the local computing and data offloading, and the strong optimization capability algorithms for inspection will be the trend in the future.

2. System Models and Methods

2.1. System Models

2.1.1. The UAV Computation System Model Assisted by MEC Server. For a computation task on the UAVs, first, we consider only one UAV local computation system here. Let D_c, t_c, f_u, C_u, ϵ_u, and E_c denote the computation data amounts in the UAV, the UAV local computation time, the CPU frequency, the number of CPU cycles to complete the computation, the effective capacitance coefficient of the CPU, and the UAV computation energy consumption, respectively; according to [12, 18–20], we have

$$t_c = \frac{(D_c C_u)}{f_u}, \tag{1}$$

$$E_c = \epsilon_u C_u D_c {f_u}^2. \tag{2}$$

In the offshore wind farm, the horizontal location of the wind turbine is denoted as $q_k = [x_k, y_k]$, $k \in \mathrm{WT}$. When the UAV detects a wind turbine, the image data of each wind turbine is indicated as D_{wt}. Part of the data is sent to the MEC server to reduce the computation burden of the UAV, where the MEC server is connected to a MEC network established by one or more LEO satellites [12, 21]. Thus, at the kth wind turbine, we have the data transmitting time from UAV to the MEC server:

$$t_k = \frac{(D_{\mathrm{wt}} - D_c)}{r_k}, \tag{3}$$

where r_k is the throughput between the MEC server and the UAV. Because the ocean environment and the distance between the UAV and the MEC server change, the throughput can be also changed with the different wind turbines detected by UAV's camera.

The computation offloading stage of the MEC server can be divided into three steps: the offloading step, the computation step, and the downloading step. Similar to [18], the time of the MEC server's computing and the UAV's download time can be ignored. Meanwhile, the MEC server can simultaneously process the image data by computation offloading and UAV local computing, likeness to [20]. Since the damages need to be fed back in real time, all image data are processed before leaving the wind turbine. For the UAV detection time dt_k (i.e., the image data processing time) at the kth wind turbine, we have

$$\mathrm{dt}_k = \max\,(t_k, t_c). \tag{4}$$

According to (4), the UAV should hover at a wind turbine and has the corresponding detection energy consumption E_d, which can be expressed as

$$E_d = E_c + P_{\mathrm{h}} * \mathrm{dt}_k + P_{uc} t_k, \tag{5}$$

where P_{uc} is the communication-related power consumption and P_{h} is the hovering energy consumption of the UAV.

2.1.2. The UAV Flight Model. As far as the UAV inspecting wind turbines is concerned, it usually faces a wind environmental condition (wind speed) on the inspection route. We consider a UAV flying system shown in Figure 1(a). The thrust T_φ of the UAV is expressed as

$$T_\varphi \cos\alpha = \mathrm{mg}, \tag{6}$$

where α is a tilt angle between the vector of T_φ and the inverse direction vector of mg and mg is the weight of the UAV in newton. The α can be obtained as follows [29]:

$$\alpha = \arctan\left(\frac{w^2}{\mu}\right), \tag{7}$$

where w is the wind speed and μ is an empirically determined coefficient with a value of 58 [29]. Therefore, a relationship between the thrust T_φ and the wind speed w is

$$T_\varphi = \frac{\mathrm{mg}}{\cos\,(\arctan\,(w^2/\mu))}. \tag{8}$$

Based on [30–32], a power consumption $P_f(V, w)$ of a UAV flying, in watt (W) as unit, is decomposed as follows:

$$\begin{aligned}\mathrm{PH}(V_{\mathrm{h}}) = {} & P_0\left(\frac{1}{V_{\mathrm{h}}} + \frac{3V_{\mathrm{h}}}{\Omega^2 {R_u}^2}\right) \\ & + (1+\gamma)T_\varphi\left(\sqrt{\frac{{T_\varphi}^2}{4{V_{\mathrm{h}}}^4\rho^2\mathrm{DA}^2} + \frac{1}{4}} - \frac{1}{2}\right)^{1/2} \\ & + \frac{1}{2}d_0\rho s * \mathrm{DA} * {V_{\mathrm{h}}}^2,\end{aligned} \tag{9}$$

where V, P_0, Ω, R_u, and γ stand for the airspeed of UAV, the constant introduced in [30], the blade angular velocity, the rotor radius, and the incremental correction factor to induced power, respectively. d_0, ρ, and s are introduced as the fuselage drag ratio, the air density, and the rotor solidity, respectively. The rotor disc area is indicated by DA.

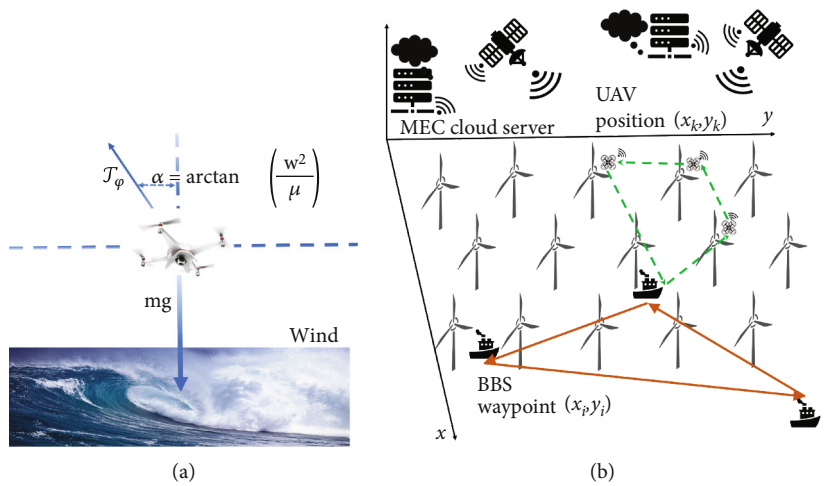

Figure 1: Two models: (a) the UAV flight model with the influence of wind; (b) the problem model.

According to (9), under the wind condition, the power consumption PH in flying is expressed as

$$\mathrm{PH} = \frac{P_f(V_\mathrm{h}, w)}{V_\mathrm{h}}, \tag{10}$$

where V_h is the horizontal speed of the UAV.

2.2. Formulation of Problem. In Figure 1(b), the waypoint of the BBS is denoted as $v_i = [x_i, y_i]$, $i \in I$. Here, I is defined as a set of the waypoints of the BBS. All wind turbines compose a set WT, which can be decomposed to I numbers of subsets WT_i. Each subset WT_i can be again decomposed to M numbers of subsets $\mathrm{WT}_{i,m}$, as well. There is a plane distance $\mathrm{PD}_{k,l} = ||q_k - q_l||, k, l \in \mathrm{WT}_{i,m}$ between any two turbines. Assuming one turbine is only inspected by the UAV once, the sum of the traveling distance of the UAV in a subset is

$$\mathrm{PD}_{Ut,i,m} = \sum_{k \in \mathrm{WT}_{i,m}}^{\mathrm{WT}_{i,m}} \sum_{l \in \mathrm{WT}_{i,m}/\{k\}}^{\mathrm{WT}_{i,m}} \mathrm{PD}_{k,l}. \tag{11}$$

Let v_i denote the starting place and the ending place of the UAV (i.e., the position of the BBS); we have

$$\mathrm{PD}_{Ut,i,m} = \sum_{k \in \mathrm{WT}_{i,m}}^{\mathrm{WT}_{i,m}} \sum_{l \in \mathrm{WT}_{i,m}/\{k\}}^{\mathrm{WT}_{i,m}} \mathrm{PD}_{k,l} \tag{12}$$

$$\text{subject to} \sum_{l \in \mathrm{WT}_{i,m}} P_{i,v_i,l} = 1, \sum_{l \in \mathrm{WT}_{i,m}} P_{i,l,v_i} = 1, l \in \mathrm{WT}_{i,m}, i \in I, v_i \subset I \tag{13a}$$

$$\sum_{k \in \mathrm{WT}_{i,m}} P_{i,k,l} = \sum_{l \in \mathrm{WT}_{i,m}} P_{i,l,k} = 1, k, l \in \mathrm{WT}_{i,m} \tag{13b}$$

$$\sum_{k \in S_u} \sum_{l \in S_u} P_{i,k,l} \le |S_u| - 1, \forall S_u \subset \mathrm{WT}_{i,m}, 2 \le |S_u| \le \left|\mathrm{WT}_{i,m}\right| - 1, \tag{13c}$$

where (13a) indicates that both the starting and ending places of the UAV are v_i. (13b) ensures only one path between the kth turbine and the lth turbine. (13c) states only one loop in the subset of $\mathrm{WT}_{i,m}$. So, the total traveling time $\mathrm{TT}_{\mathrm{Utra}}$ of the UAV in the inspection of all the wind turbines is expressed as

$$\mathrm{TT}_{\mathrm{Utra}} = \frac{\sum_{i=1}^{I} \sum_{m=1}^{M} \mathrm{PD}_{Ut,i,m}}{V_\mathrm{h}}. \tag{14}$$

For each subset $\mathrm{WT}_{i,m}$, the sum $(E_{i,m})$ of energy consumption of detecting wind turbines is expressed as

$$E_{i,m} = \sum_{k \in \mathrm{WT}_{i,m}}^{\mathrm{WT}_{i,m}} E_{d,k}. \tag{15}$$

As shown in Figure 1(b), for a waypoint set of the BBS in the wind farm, there is a plane distance $\mathrm{PD}_{i,j} = ||v_i - v_j||, i, j \in I$ between two waypoints. So, the total traveling distance of the BBS is

$$\mathrm{PD}_{\mathrm{BBS}} = \sum_{i \in I}^{I} \sum_{j \in I/\{i\}}^{I} \mathrm{PD}_{i,j}. \tag{16}$$

Let B_{SE} denote the starting and ending places of the BBS; each waypoint is only visited once, and we have

$$\mathrm{PD}_{\mathrm{BBS}} = \sum_{i \in I}^{I} \sum_{j \in I/\{i\}}^{I} \mathrm{PD}_{i,j} \tag{17}$$

$$\text{subject to} \sum_{j \in I} P_{B_{\mathrm{SE}},j} = 1, \sum_{j \in I} P_{j,B_{\mathrm{SE}}} = 1, j \in I, B_{\mathrm{SE}} \subset I \tag{18a}$$

$$\sum_{i \in I} P_{i,j} = \sum_{j \in I} P_{i,j} = 1, i, j \in I \tag{18b}$$

$$\sum_{i\in S_B}\sum_{j\in S_B} P_{i,j} \le |S_B| - 1, \forall S_B \subset I, 2 \le |S_B| \le |I| - 1, \tag{18c}$$

where (18a) indicates that both the starting and ending places of the BBS are B_{SE}. (18b) ensures only one path between the ith waypoint and the jth waypoint (i.e., the orange line). (18c) states only one loop in the set of I.

Let V_{BBS} denote the velocity of the BBS, and the traveling time $\mathrm{TT}_{\mathrm{BBS}t}$ of the BBS in the inspection of the wind farm is expressed as

$$\mathrm{TT}_{\mathrm{BBS}t} = \frac{\mathrm{PD}_{\mathrm{BBS}}}{\mathrm{V}_{\mathrm{BBS}}}. \tag{19}$$

Let P_{BBS} denote the propulsion load of the BBS, and then, for minimizing the total inspection energy consumption E_t in the offshore wind farm, we have Problem 1. Problem 1 is expressed as

Problem 1.

$$\min_{k,l\in \mathrm{WT},i,j\in I} E_t = \min_{k,l\in \mathrm{WT}} \sum_{i=1}^{I}\sum_{m=1}^{M} E_{i,m} + \sum_{i=1}^{I}\sum_{m=1}^{M} \mathrm{PD}_{Ut,i,m}\mathrm{PH} + \mathrm{P}_{\mathrm{BBS}}\mathrm{TT}_{\mathrm{BBS}t} \tag{20}$$

$$\text{subject to } \sum_{l\in \mathrm{WT}_{i,m}} P_{i,v_i,l} = 1, \sum_{l\in \mathrm{WT}_{i,m}} P_{i,l,v_i} = 1, l \in \mathrm{WT}_{i,m}, i \in I, v_i \subset I \tag{21a}$$

$$\sum_{k\in \mathrm{WT}_{i,m}} P_{i,k,l} = \sum_{l\in \mathrm{WT}_{i,m}} P_{i,l,k} = 1, k, l \in \mathrm{WT}_{i,m} \tag{21b}$$

$$\sum_{k\in S_u}\sum_{l\in S_u} P_{i,k,l} \le |S_u| - 1, \forall S_u \subset \mathrm{WT}_{i,m}, 2 \le |S_u| \le \left|\mathrm{WT}_{i,m}\right| - 1 \tag{21c}$$

$$\sum_{j\in I} P_{B_{\mathrm{SE}},j} = 1, \sum_{j\in I} P_{j,B_{\mathrm{SE}}} = 1, j \in I, B_{\mathrm{SE}} \subset I \tag{21d}$$

$$\sum_{i\in I} P_{i,j} = \sum_{j\in I} P_{i,j} = 1, i, j \in I \tag{21e}$$

$$\sum_{i\in S_B}\sum_{j\in S_B} P_{i,j} \le |S_B| - 1, \forall S_B \subset I, 2 \le |S_B| \le |I| - 1. \tag{21f}$$

In order to simulate the limitation of the UAV battery capacity, there are still some constraints in Problem 1 as follows:

(i) The limitation of energy consumption assigned to UAV flying, i.e., $\mathrm{PD}_{Ut,i,m}\mathrm{PH} \le E_{\mathrm{UtraL}}$

(ii) The limitation of energy consumption assigned to UAV detecting, i.e., $E_{i,m} \le E_{\mathrm{UdetL}}$. Therefore, Problem 1 is rewritten as

Problem 2.

$$\min_{k,l\in \mathrm{WT},i,j\in I} E_t = \min_{k,l\in \mathrm{WT}} \sum_{i=1}^{I}\sum_{m=1}^{M} E_{i,m} + \sum_{i=1}^{I}\sum_{m=1}^{M} \mathrm{PD}_{Ut,i,m}\mathrm{PH} + \mathrm{P}_{\mathrm{BBS}}\mathrm{TT}_{\mathrm{BBS}t} \tag{22}$$

$$\text{subject to (21a)—(21f)} \tag{23a}$$

$$\mathrm{PD}_{Ut,i,m}\mathrm{PH} \le E_{\mathrm{UtraL}} \tag{23b}$$

$$E_{i,m} \le E_{\mathrm{UdetL}}. \tag{23c}$$

For the set WT, the total detection time $\mathrm{TT}_{\mathrm{Udet}}$ in the offshore wind farm is expressed as

$$\mathrm{TT}_{\mathrm{Udet}} = \sum_{i=1}^{I}\sum_{m=1}^{M}\sum_{k\in \mathrm{WT}_{i,m}}^{\mathrm{WT}_{i,m}} \mathrm{dt}_k. \tag{24}$$

In summary, the total inspection time T_{ti} in the wind farm can be expressed as

$$T_{\mathrm{ti}} = \mathrm{TT}_{\mathrm{Utra}} + \mathrm{TT}_{\mathrm{BBS}t} + \mathrm{TT}_{\mathrm{Udet}}. \tag{25}$$

Thus, to find the minimum total inspecting time in the offshore wind farm under the MEC- and BBS-assisted UAV, the minimization problem can be formulated as

Problem 3.

$$\min_{i,j\in I,k,l\in \mathrm{WT}} T_{\mathrm{ti}} = \min_{i,j\in I,k,l\in \mathrm{WT}} \mathrm{TT}_{\mathrm{Utra}} + \mathrm{TT}_{\mathrm{BBS}t} + \mathrm{TT}_{\mathrm{Udet}} \tag{26}$$

$$\text{subject to (21a)—(23c)} \tag{27}$$

2.3. Solution of Problem. Solving Problem 1 is decomposed into four simple subproblems, and then, Problem 3 can be addressed according to the answer to Problem 1.

2.3.1. Minimizing the UAV Detection Time in One Wind Turbine. To minimize E_t in the offshore wind farm, according to the constraints (23c) and (15), in the detection energy consumption $E_{d,k}$ in (5), there is the first simple subproblem, i.e., minimizing the detection time (dt_k) of detecting one wind turbine. Therefore, for the detection time, according to (1), (3), and (4), dt_k can be rewritten as

$$\mathrm{dt}_k = \max\left(\frac{D_c C_u}{f_u}, \frac{(D_{wt} - D_c)}{r_k}\right). \tag{28}$$

So, we have Proposition 4.

Proposition 4. *If a local minimum exists in the dt_k, it is the only local minimum in dt_k.*

Proof. Let $f(D_c) = D_c C_u / f_u$, and then, it is easy to find out that $f(D_c)$ is a single increasing function with D_c. Let $g(D_c) = (D_{wt} - D_c)/r_k$, and then, it is easy to find out that $g(D_c)$

is a single decreasing function with D_c. When $f(\min D_c) < g(\min D_c)$ and $f(\max D_c) > g(\max D_c)$, the minimum dt_k exists when $f(D_c) = g(D_c)$.

When the hovering energy consumption (P_{h}) of the UAV is much larger than the communication-related power consumption (P_{uc}) and the UAV computation energy consumption (E_c), the minimum value of the $E_{d,k}$ is decided by dt_k. □

2.3.2. Minimizing Flight Power Consumption of the UAV. According to constraints (23b) and (10), the second simple subproblem, i.e., the minimum flight power consumption (PH) of the UAV, can be found. Then, we have Proposition 5.

Proposition 5. *If a local minimum exists in the $P_f(V_h, w)/V_h$ and when $V_h > 0$, it is the only local minimum of the function.*

Proof. Define $\mathrm{PH}(V_{\mathrm{h}}) = P_f(V_{\mathrm{h}}, w)/V_{\mathrm{h}}$; we have

$$\begin{aligned}\mathrm{PH}(V_{\mathrm{h}}) = {} & P_0\left(\frac{1}{V_{\mathrm{h}}} + \frac{3V_{\mathrm{h}}}{\Omega^2 {R_u}^2}\right) \\ & + (1+\gamma)T_\varphi\left(\sqrt{\frac{{T_\varphi}^2}{4{V_{\mathrm{h}}}^4\rho^2\mathrm{DA}^2} + \frac{1}{4}} - \frac{1}{2}\right)^{1/2} \\ & + \frac{1}{2}d_0\rho s * \mathrm{DA} * {V_{\mathrm{h}}}^2.\end{aligned} \tag{29}$$

We must show $\mathrm{PH}(V_{\mathrm{h}})$ being concave (i.e., $\partial \mathrm{PH}^2(V_{\mathrm{h}})/\partial {V_{\mathrm{h}}}^2 > 0$). It is easy to prove that the first and third terms are both concave. For the second term, define $\gamma^2 = {T_\varphi}^2/\rho^2 \mathrm{DA}^2$. According to the first-order Taylor approximation, when $\gamma^2/{V_{\mathrm{h}}}^4 \ll 1$, we have

$$\begin{aligned}(V_{\mathrm{h}}) \triangleq {} & \left(\sqrt{\frac{\gamma^2}{4{V_{\mathrm{h}}}^4} + \frac{1}{4}} - \frac{1}{2}\right)^{1/2} = \frac{\sqrt{2}}{2}\left(\sqrt{\frac{\gamma^2}{{V_{\mathrm{h}}}^4} + 1} - 1\right)^{1/2} \\ = {} & \frac{\sqrt{2}}{2}\left(\frac{\gamma^2}{2{V_{\mathrm{h}}}^4} + 1 - 1\right)^{1/2} = \frac{1}{2}\frac{\gamma}{{V_{\mathrm{h}}}^2}.\end{aligned} \tag{30}$$

It is easy to prove $(1+\gamma)T\varphi\, g(V_{\mathrm{h}}) > 0$. A nonnegative, nonzero weighted sum of strictly concave function is strictly concave. So, $\mathrm{PH}(V_{\mathrm{h}})$ is concave when $V_{\mathrm{h}} > 0$. □

2.3.3. Minimizing the Total UAV Traveling Distance in Inspecting the Offshore Wind Farm. After minimizing the corresponding detection energy consumption ($E_{d,k}$) and the flight power consumption of the UAV (PH), the next objective is to minimize the total traveling distance of the UAV in the inspection of all the wind turbines. For this, according to the subset $\mathrm{WT}_{i,m}$, the constraint (23b), and the constrain (23c), the minimization problem is expressed as

Problem 6.

$$\min_{i\in I}\sum_{i=1}^{I}\sum_{m=1}^{M}\mathrm{PD}_{Ut,i,m} \tag{31}$$

$$\text{subject to (18a)—(18c)} \tag{32a}$$

$$\mathrm{PD}_{Ut,i,m}\mathrm{PH} \le E_{\mathrm{UtraL}} \tag{32b}$$

$$E_{i,m} \le E_{\mathrm{UdetL}}. \tag{32c}$$

According to the constraints, Problem 6 is transformed into a DCVRP. So, Problem 6 is obviously a strongly NP-hard problem. The methods of solving DCVRP are diverse. It can be used on any one of the algorithms as follows: LKH-3, genetic algorithm (GA), ant colony optimization (ACO) algorithm, simulated annealing (SA), and particle swarm optimization (PSO). Here, we use LKH-3 to find a promising DCVRP solution, for conveniently addressing Problem 6.

2.3.4. Minimizing the BBS Traveling Time in Inspecting the Offshore Wind Farm. For the traveling time $\mathrm{TT}_{\mathrm{BBS}t}$ of the BBS in the inspection of the wind farm, its minimization problem is expressed as

Problem 7.

$$\min_{i,j\in I}\mathrm{TT}_{\mathrm{BBS}t} \tag{33}$$

$$\text{subject to (21d)—(21f)} \tag{34}$$

Although Problem 7 is a simple TSP problem, the problem size of Problem 7 increases with the increment of the number i of the subset WT_i, $i \in I$.

In summary, according to Proposition 4, Proposition 5, Problem 6, and Problem 7, E_t can be minimized. For this, a heuristic algorithm is designed to solve the minimum total inspection energy consumption problem. In addition, according to (28), (31), and (33), the minimum total inspecting time (i.e., Problem 3) also can be solved.

2.4. Algorithm Design. Based on Proposition 4, Proposition 5, Problem 6, and Problem 7, the new heuristic algorithm (i.e., MOA) is designed based on the K-means, SEC, and LKH-3 to address Problem 1.

2.4.1. Algorithm 1: MOA. For the given wind turbine locations (i.e., the set WT) in the offshore wind farm, to optimize the total inspecting energy consumption to minimal value by the algorithm, MOA, obtaining the optimal positions of the BBS waypoint is crucial.

Therefore, the steps of the MOA to address Problem 1 are arranged as follows:

(i) The waypoints $\{v_1, \cdots, v_I\}$ of the BBS are obtained by K-means algorithm and SEC algorithm. Then, the offshore wind farm WT is divided into multiple subsets WT_i by the distance $\mathrm{PD}_{i,k}$ between the waypoint of BBS and the location of the wind turbine

Input: WT, I, V_{BBS}, P_{BBS}, P_u, P_{uc}, PH, D_{wt}, r_k
Output: E_t, T_{ti}
1. The waypoints $\{v_1,\cdots,v_I\}$ and the subsets $\{\mathrm{WT}_1,\cdots,\mathrm{WT}_\mathrm{I}\}$ are obtained by K-means algorithm and SEC algorithm;
2. for i =1 to I
3. Obtain the sum of UAV detecting times $\sum_{m=1}^{M}\sum_{k\in WT_{i,m}}^{WT_{i,m}} dt_k$ and the sum of UAV detecting energy consumption $\sum_{m=1}^{M} E_{i,m}$in one subset WT_i;
4. Obtain the sum of UAV traveling energy consumption $\sum_{m=1}^{M} PD_{Ut,i,m}PH$ by LKH-3with v_i, WT_i, E_{UtraL}, and E_{UdetL};
5. end
6. Obtain the traveling distance PD_{BBS} of the BBS by LKH
7. $TT_{BBSt} \longleftarrow PD_{BBS}/V_{BBS}$;
8. $E_t \longleftarrow \sum_{i=1}^{I}\sum_{m=1}^{M} E_{i,m} + \sum_{i=1}^{I}\sum_{m=1}^{M} PD_{Ut,i,m}PH + P_{BBS}TT_{BBSt}$;
9. $TT_{Udet} \longleftarrow \sum_{i=1}^{I}\sum_{m=1}^{M}\sum_{k\in WT_{i,m}}^{WT_{i,m}} dt_k$;
10. $TT_{Utra} \longleftarrow \sum_{i=1}^{I}\sum_{m=1}^{M} PD_{Ut,i,m}/V_U$;
11. $T_{ti} \longleftarrow TT_{Utra} + TT_{BBSt} + TT_{Udet}$.

Algorithm 1: Mixed optimization algorithm (MOA).

(ii) For each subset WT_i, using the BBS waypoints as the UAV starting and ending places, under the limitation of energy consumption assigned to UAV for flying E_{UtraL} and detecting E_{UdetL}, the sum of traveling distance in one subset is obtained. Then, the total traveling distance is also acquired (i.e., Problem 6)

(iii) The traveling time of the BBS is obtained by the LKH (i.e., Problem 7)

The details in Algorithm 1 are given as follows.

So, the time complexity analysis of the MOA can be analyzed as follows: for the K-means cluster algorithm, we assume that the number of iterations is iter. The time complexity of the K-means algorithm is $O(2|I||\mathrm{WT}|\mathrm{iter})$ in line 1. Meanwhile in line 1, according to [33], the time complexity of the SEC algorithm is $O(|I|\ \lg(\mathrm{md}/\mathrm{Ra})|\mathrm{WT}_i|)$, where md is the shortest distance from a point to the circumference of a circle when the point is outside the circle and Ra is the radius of the smallest circle that we need to obtain in the last round of iteration.

In Problem 6, the time complexity of the LKH-3 can be simplified to $O(|\mathrm{WT}_i|)$. Problem 7 is similar to Problem 6; the time complexity of the solution in Problem 7 is $O(|I|)$. In a word, in the MOA, the LKH-3 needs to run $|I|$ times. From the discussions above, the time complexity of MOA is $O(2|I||\mathrm{WT}|\mathrm{iter}) + O(|I|\ \lg(\mathrm{md}/\mathrm{Ra})|\mathrm{WT}_i|) + O(|I||\mathrm{WT}_i|) + O(|I|^2)$.

3. Results and Discussion

To comprehensively evaluate the performance of MOA in solving Problem 1 and Problem 3, i.e., under the MEC- and BBS-assisted UAV, minimizing the total inspecting energy consumption and total inspecting time for the offshore wind farm, numerical results are provided by simulations. The physical meaning and values of the parameters are given in Table 1. Under wind conditions, to simulate the hovering energy consumption system of the UAV, the parameters and their physical meanings of the UAV are also shown in Table 1. The parameter values are based on the specification values of the UAV used in the simulation. For simulating each pair of wind turbine's realistic distance from each other, its coordinate is quoted from kingfisher information service-offshore renewable cable awareness (KIS-ORCA) [1]. A plane coordinate of a wind turbine transforms from the longitude and the latitude via a transformation program called PROJFWD in MATLAB. All the simulations are conducted in MATLAB 2020b. The as-simulation results are analyzed and discussed as follows.

To clearly illustrate the performance of the as-proposed scheme, we compare it with the following schemes:

(i) Full MEC server computation scheme (FSC): all data is transmitted to the MEC server for computation [18]

(ii) Full UAV local computation scheme (FULC): all data is computed in the local UAV [12]

3.1. Discussion of Proposition 4 and Proposition 5. Two simulating numerical data results of Proposition 4 and Proposition 5 are shown in Figures 2(a) and 2(b), respectively. Figure 2(a) shows the relations between the throughput and the corresponding detection energy consumption under different computation schemes. In Proposition 4, the FULC and the FSC indicate that $D_c = D_{\mathrm{wt}}$ and $D_c = 0$ in (3), respectively. From Figure 2(a), the corresponding detection energy consumption decreases with the throughput increment between the MEC server and the UAV in the as-proposed computation scheme and the FSC scheme. The energy consumption remains unchanged with the throughput increment in the FULC scheme. When the throughput is smaller than 18 Mbit/s, the corresponding detection energy consumption in the as-proposed scheme is the smallest among the three schemes. At this time, it means that it is better that part of the data is transmitted from the UAV to

Table 1: Parameters and their values.

Parameters	Physical meaning	Value
E_{UtraL}	Maximum traveling energy limitation of the UAV	90 kJ
E_{UdetL}	Maximum detection energy limitation of the UAV	60 kJ
V_{BBS}	Speed of BBS	5 m/s
P_{BBS}	The propulsion load of the BBS [34]	120 kW
P_{h}	The power consumption of UAV in hovering	181.32 W
P_{uc}	The communication power consumption	5 W
h	The UAV's average communication altitude	110 m
C_u	The number of CPU cycles to complete the computation	10^3 cycles/bit
ϵ_u	The effective capacitance coefficient of the CPU	10^{-28}
f_u	The CPU frequency	10 GHz
mg	Aircraft weight in newton	20
ρ	Air density in kg/m^3	1.225
R_u	Rotor radius in meter (m)	0.4
DA	Rotor disc area in m^2, DA $\triangleq \pi {R_u}^2$	0.503
Ω	Blade angular velocity in radians/second	300
N_b	Number of blades	4
B_l	Blade or aerofoil chord length	0.0157
s	Rotor solidity, defined as the ratio of the total blade area to the disc area, $s \triangleq N_b B_l/\pi R_u$	0.05
S_{FP}	Fuselage equivalent fat plate area in m^2	0.0151
d_0	Fuselage drag ratio, defined as $d_0 = S_{\mathrm{FP}}/s\mathrm{DA}$	0.6
γ	Incremental correction factor to induced power	0.1
ϑ	Profile drag coefficient	0.012
$T\varphi$	Rotor thrust	

the MEC server for computation. When the throughput is over 18 Mbit/s, the energy consumption in FSC is the same as that in the as-proposed scheme, and the energy consumption in the both schemes is lower than that in FULC. It means that the larger the throughput, the better using the MEC server for computation.

Figure 2(b) shows under different average wind speeds, the relation between the proposed computation scheme's power consumption, and the airspeed of the UAV (V_{h} m/s). Here, five different average wind speeds ($\omega = [6, \cdots, 10\,\mathrm{m/s}]$) are provided by [1]. When the airspeed $V_{\mathrm{h}} = 5$, the power consumption is the highest. Then, the power consumption decreases as the airspeed increases from $V_{\mathrm{h}} = 5$ to 15. However, the power consumption increases as the airspeed increases from 25 to 30. When the airspeed (V_{h}) increases from 15 to 25, the lowest power consumption points emerge on each power consumption line. Therefore, there is an optimal airspeed corresponding to the minimum power consumption in each average wind speed. The optimal values for power consumption shown in Figure 2(b) are listed in Table 2. In offshore wind farm inspection, the minimum power consumption of the UAV flight is crucial to saving energy and increasing the efficiency of the UAV inspection.

3.2. The Result Comparison of Schemes under Different Data Amounts. For evaluating the performance of the as-proposed scheme, under the different image data amounts, the boat-direct, the FSC, and the FULC are employed to compare with the as-proposed. The boat-direct uses a boat (BBS) to carry a UAV directly to each wind turbine position for detection, where it follows a TSP route. Figure 3(a) shows the comparison results of E_t under different data amounts in four schemes. There, E_t of the four schemes increases with the increment of the data amount. While compared with the other three schemes, the as-proposed scheme has the smallest E_t. Compared especially to the boat-direct, the E_t gap is about 44% on average. It means that approximately 44% of energy consumption can be saved on average, relative to boat-direct. The reason for presenting a large energy consumption gap between the as-proposed and the boat-direct is that the as-proposed scheme has a minimum traveling distance. Although when the data amount is 100 Mbit, E_t of the three (i.e., the as-proposed, the FULC, and the FSC) is quite close; when the data amount increases, the E_t gap in the three schemes becomes bigger and bigger. When the data amount is 1000 Mbit, the as-proposed can save about 0.12% and 0.06% energy consumption, relative to the FULC and the FSC, respectively. We can conclude from Figure 3(a) that

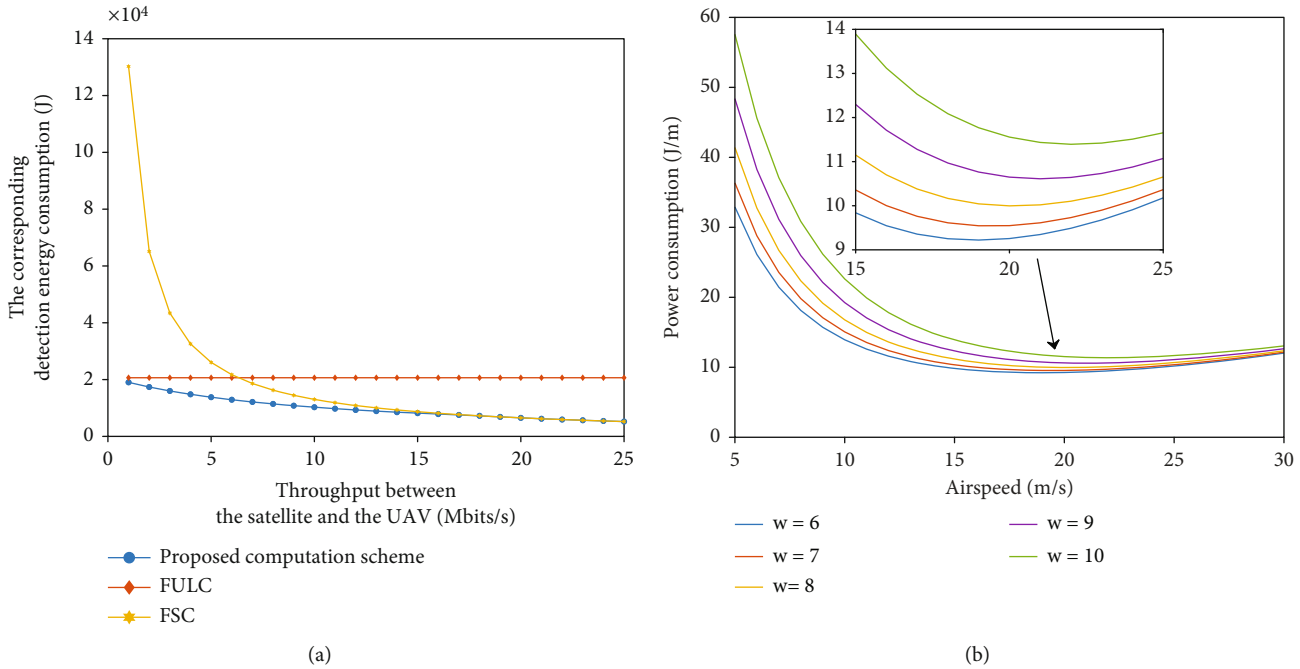

Figure 2: (a) Changes in the detection energy consumption with the throughput under different computation schemes. (b) Variation in the proposed computation scheme's power consumption with the UAV airspeed (V_h), under different average wind speeds.

Table 2: Optimal airspeed and power consumption under different wind speeds.

Average wind speed W (m/s)	Airspeed of UAV V_h (m/s)	Power consumption (J/m)
6	19	9.22
7	19	9.54
8	20	9.99
9	21	10.61
10	23	11.39

the as-proposed scheme achieved the objective of saving energy under the data amount increasing condition, and this gain is quite remarkable when the collected data amount is more and more, especially for the future of developing super large-scale wind farm towards the wider and deep sea.

To arrive at the aim of saving energy and high-efficient inspection, we also investigate the total inspection time (T_{ti}) in four schemes. Figure 3(b) shows the comparison results of four schemes of T_{ti} under different data amounts. In Figure 3(b), T_{ti} all increase with the increment of the data amounts for four schemes. It is reasonable since the time taken for data computation increases along with data amounts. Compared with the other three, the as-proposed scheme spends the least total inspection time. Although when the data amount is 100 Mbit, T_{ti} of the three (excluding boat-direct scheme) is quite close; when the data amount increases more and more, the T_{ti} gap in our scheme relative to the other two becomes bigger and bigger. However, when the data amount increases, the T_{ti} gap between the proposed scheme and the boat-direct slightly reduces. Even so, when the data amount is 1000 Mbit, the least T_{ti} gap is still about 15%; it means that still about 15% of the T_{ti} can be saved by the as-proposed scheme relative to boat-direct. Compared to the FULC and the FSC, the as-proposed can save approximately 23% and 22%, respectively, of the T_{ti}. From Figure 3(b), it can be concluded that the as-proposed scheme is high efficient at the T_{ti} aspect under the different data amount conditions.

3.3. Comparing the Results of the Different Schemes under Different Average Wind Conditions. In the offshore wind farm, as far as evaluating the performance of the inspection scheme is concerned, the effect of average wind speed on E_t is also an important reference. According to [1], the average wind speed data range is 6 to 10 m/s, which occupies most. Figure 4(a) shows the comparison results of E_t in four schemes, and in the figure, for all the schemes, there is an insignificant change in E_t with the average wind speeds. The propulsion load of the BBS is the main power consumption in the inspection. Thus, the total energy consumption in the as-proposed, FSC, and FULC schemes is far less than that in the boat-direct. And the as-proposed scheme has the minimum total energy consumption. The as-proposed can save, on average, approximately 0.06%, 0.02%, and 41% of E_t compared to the FULC, the FSC, and the boat-direct, respectively. The objective of saving energy is achieved at different average wind speeds.

For the saving energy and high-efficient inspection at different average wind speeds, we also investigate T_{ti} in four schemes. Figure 4(b) shows the comparison results of T_{ti}; as far as the other three schemes are concerned, with the

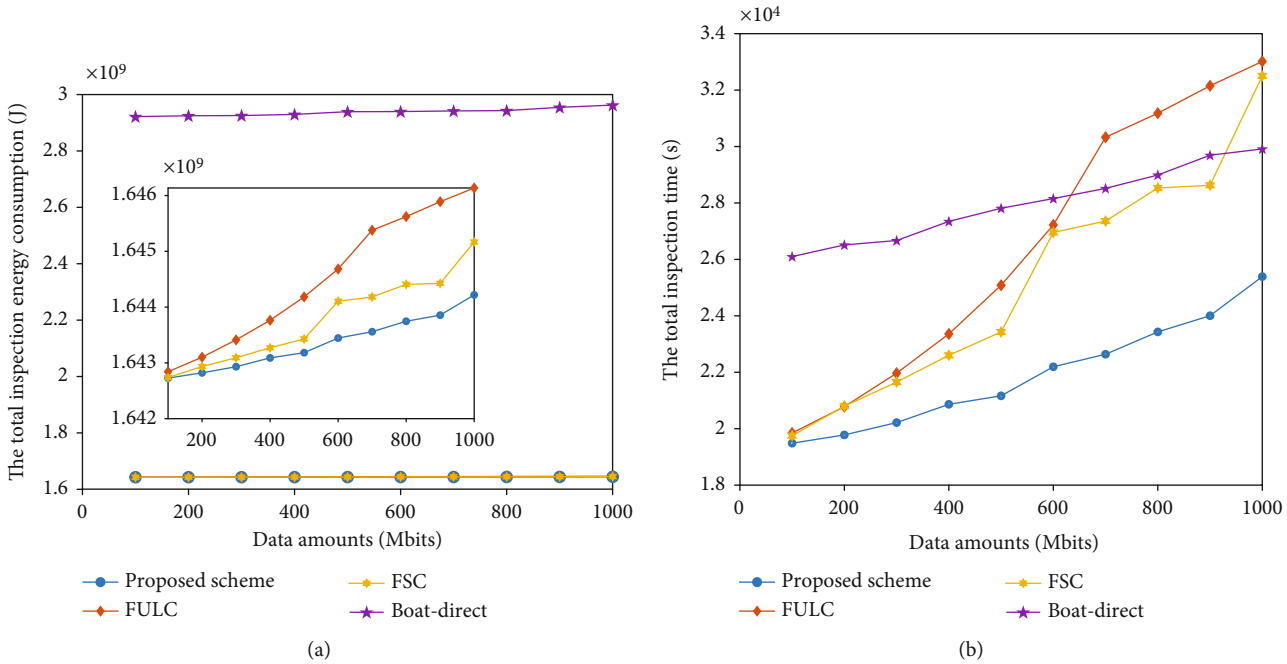

Figure 3: (a) Comparison in total inspection energy consumption for four schemes under different data amounts. (b) Comparison in total inspection time under different data amounts for four schemes.

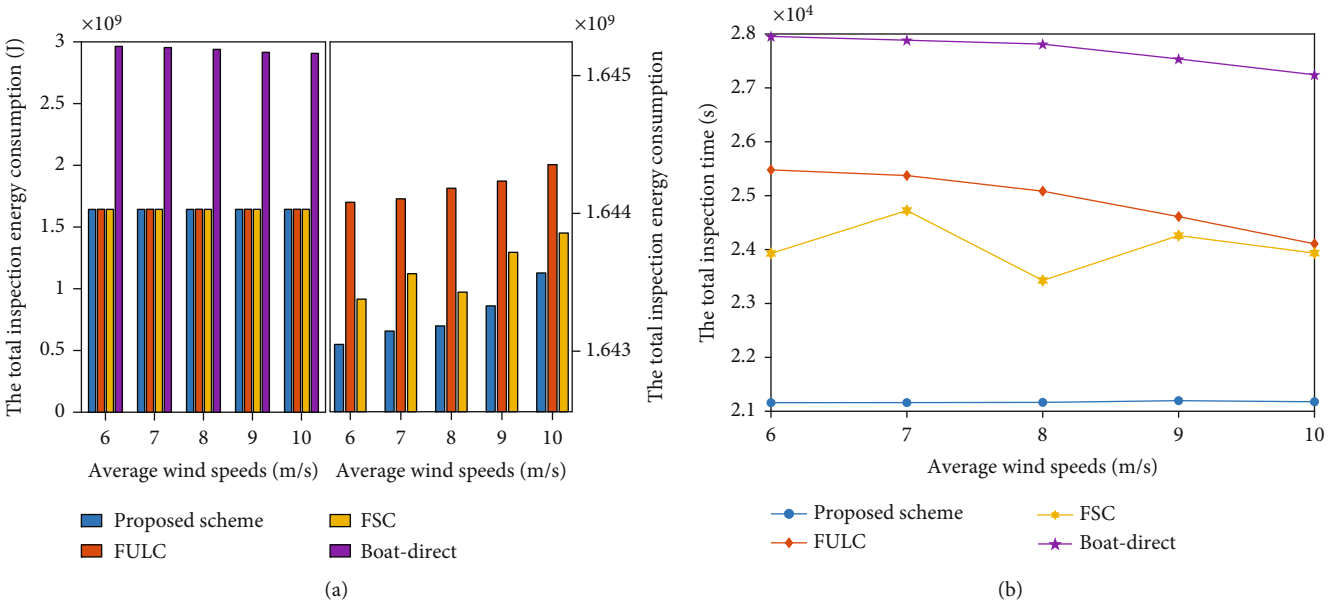

Figure 4: (a) The total inspection energy consumption for four schemes at different average wind speeds. (b) The total inspection time for four schemes at different average wind speeds.

increment of the average wind speed, there is a crucial decrement in T_{ti}. However, for the as-proposed, T_{ti} is almost unchanged. This indicates that for the usual average wind speeds, the T_{ti} obtained by simulating calculation via the as-proposed scheme is more stable and reliable, relative to those T_{ti} of the other three schemes. In the meantime, compared to the other three, T_{ti} in the proposed scheme is still the smallest. About 23.5%, 15.1%, and 11.9% time on average can be saved relative to the boat-direct, FULC, and FSC schemes, respectively. This means that the objective of the high-efficient inspection achieves at different average wind speeds.

The above accomplishments of saving energy and high-efficient inspection should be attributed to this reasonable

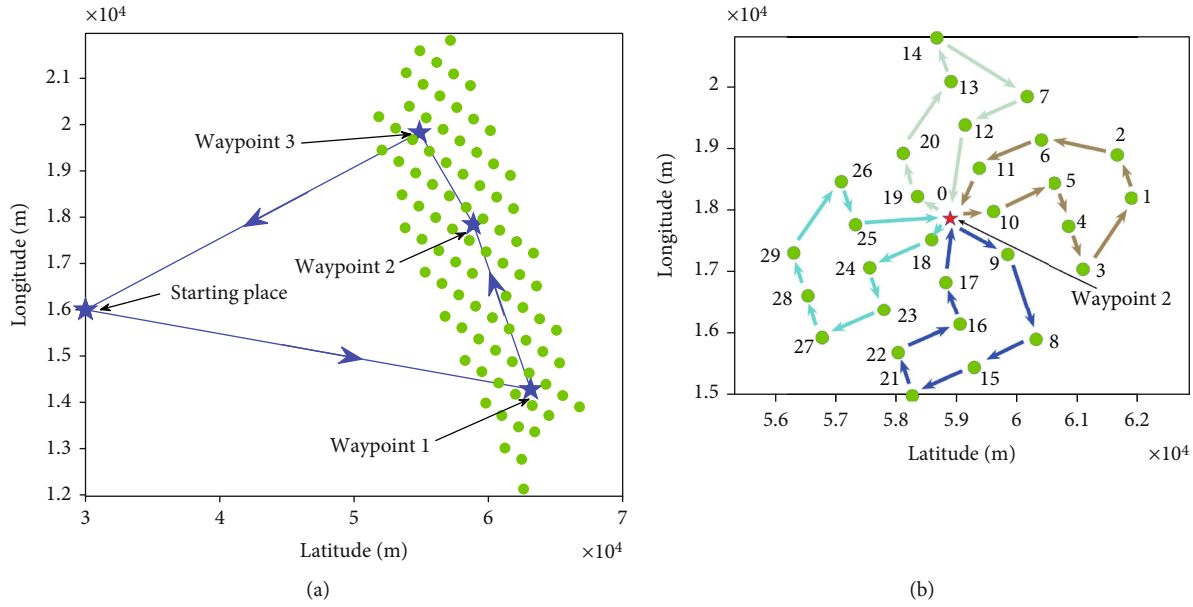

Figure 5: The inspection route of the BBS and the UAV in MOA: (a) BBS and (b) UAV at BBS waypoint 2.

scheme design, the suitable MOA, and its optimal planning routes of the boat and the UAV under LEO satellite MEC service and boat-assisted inspection shown as follows.

3.4. The Optimized Inspection Routes. Based on the results above discussion, the optimal routes of the BBS and the UAV in the as-proposed scheme (i.e., MOA) are given in this part. An interesting inspection region in the offshore wind farm is considered, where there are 86 wind turbines deployed. The unified deployment of the wind turbines is shown in Figure 5(a). A green point is the wind turbine position. A blue pentagram indicates a waypoint of the BBS. In Figure 5(a), following the direction of the blue arrow can achieve the BBS route, and the objective of saving energy and high-efficient inspection can arrive. Meanwhile, the objective achievement is also inseparable from the UAV route. Figure 5(b) shows the inspection route of the UAV in the BBS waypoint 2. At each waypoint, the BBS acts as the take-off and landing locations of the UAV. At waypoint 2, the UAV must inspect all wind turbines using four trips (see 4 different color closing lines). These trips are $0 > 19 > 20 > 13 > 14 > 7 > 12 > 0$, $0 > 18 > 24 > 23 > 27 > 28 > 29 > 26 > 25 > 0$, $0 > 10 > 5 > 4 > 3 > 1 > 2 > 6 > 11 > 0$, and $0 > 9 > 8 > 15 > 21 > 22 > 16 > 17 > 0$; the corresponding traveling distances are 8068.56 m, 8679.64 m, 8885.58 m, and 8524.52 m, respectively. The sum of traveling distance is equal to 34158 m. At the other two waypoints 1 and 3, the UAV needs to visit the wind turbine position with the five trips and the three trips (5 and 3 different color closing lines), respectively. The sum of traveling distance is 39014 m and 32547 m.

Briefly, the optimal route of the BBS, the optimal planning route of the UAV, and the minimum total inspection energy consumption (and time) of the BBS and the UAV are obtained using the MOA in our scheme.

4. Conclusions

Facing the limitations of current assisted UAV inspection of offshore wind farms, this paper proposes a new comprehensive-assisted UAV automated inspection scheme. Its objectives are conducting the saving energy and high-efficient inspection and are used for formulating two combinatorial optimization problems based on the UAV and BBS routing planning. We have solved the two problems by exploiting the new improved heuristic algorithm (MOA), made of the LKH-3, SEC, and K-means clustering algorithms, i.e., decomposing the two problems into four subproblems, and then, to be solved. First, the boat waypoints are obtained by the K-means algorithm and the SEC algorithm. Then, the offshore wind farm is divided into multiple subsets via the distance between the waypoint and the location of turbine; two sums about the drone inspecting time and the detecting energy consumption are acquired, respectively. Second, the drone total traveling distance in one subset is obtained by the LKH-3 algorithm. Third, the boat traveling distance is obtained by the LKH. Finally, we conduct simulations and use the results to comprehensively evaluate the performance of the proposed scheme. The simulation experimental results demonstrate that compared with the other three schemes, the as-proposed scheme not only has the smallest total inspection energy consumption and the least total inspection time but also, via the scheme algorithm, provides the optimal routes with the BBS and the UAV, in inspection of the offshore wind farm. These results can provide the inspecting offshore wind farms with some references. Hereafter, the ocean sensor will be studied.

Data Availability

Data is included in the article, and further inquiries can be directed to the first or corresponding author.

Conflicts of Interest

The authors declare that there is no conflict of interest regarding the publication of this paper.

Acknowledgments

This research was funded by the National Natural Science Foundation of China (grant number 62062007).

References

[1] H. M. Chung, S. Maharjan, Y. Zhang, and K. Strunz, "Placement and routing optimization for automated inspection with unmanned aerial vehicles: a study in offshore wind farm," *IEEE Transactions on Industrial Informatics*, vol. 17, no. 5, pp. 3032–3043, 2021.

[2] D. Li, S. M. Ho, G. Song, L. Ren, and H. Li, "A review of damage detection methods for wind turbine blades," *Smart Materials and Structures*, vol. 24, no. 3, article 033001, 2015.

[3] W. Qiao and D. Lu, "A survey on wind turbine condition monitoring and fault diagnosis—part I: components and subsystems," *IEEE Transactions on Industrial Electronics*, vol. 62, no. 10, pp. 6536–6545, 2015.

[4] K. Branner and A. Ghadirian, "Database about blade faults," DTU Wind Energy E-0067, Technical Report, 2014.

[5] X. Yang, Y. Zhang, W. Lv, and D. Wang, "Image recognition of wind turbine blade damage based on a deep learning model with transfer learning and an ensemble learning classifier," *Renewable Energy*, vol. 163, pp. 386–397, 2021.

[6] X. Huang, G. Wang, Y. Lu, and Z. Jia, "Study on a boat-assisted drone inspection scheme for the modern large-scale offshore wind farm," *IEEE Systems Journal*, vol. 17, no. 3, pp. 4509–4520, 2023.

[7] B. Alzahrani, O. S. Oubbati, A. Barnawi, M. Atiquzzaman, and D. Alghazzawi, "UAV assistance paradigm: state-of-the-art in applications and challenges," *Journal of Network and Computer Applications*, vol. 166, article 102706, 2020.

[8] A. Qayyum, I. Ahmad, M. Iftikhar, and M. Mazher, "Object detection and fuzzy based classification using UAV data," *Intelligent Automation & Soft Computing*, vol. 26, no. 4, pp. 693–702, 2020.

[9] L. Wang and Z. Zhang, "Automatic detection of wind turbine blade surface cracks based on UAV-taken images," *IEEE Transactions on Industrial Electronics*, vol. 64, no. 9, pp. 7293–7303, 2017.

[10] L. Wang, Z. Zhang, and X. Luo, "A two-stage data-driven approach for image-based wind turbine blade crack inspections," *IEEE/ASME Transactions on Mechatronics*, vol. 24, no. 3, pp. 1271–1281, 2019.

[11] D. Xu, C. Wen, and J. Liu, "Wind turbine blade surface inspection based on deep learning and UAV-taken images," *Journal of Renewable and Sustainable Energy*, vol. 11, no. 5, article 053305, 2019.

[12] P. Cao, Y. Liu, C. Yang, S. Xie, and K. Xie, "MEC-driven UAV-enabled routine inspection scheme in wind farm under wind influence," *IEEE Access*, vol. 7, pp. 179252–179265, 2019.

[13] H. Baik and J. Valenzuela, "An optimization drone routing model for inspecting wind farms," *Soft Computing*, vol. 25, no. 3, pp. 2483–2498, 2021.

[14] A. Thibbotuwawa, G. Bocewicz, G. Radzki, P. Nielsen, and Z. Banaszak, "UAV mission planning resistant to weather uncertainty," *Sensors*, vol. 20, no. 2, p. 515, 2020.

[15] D. Xu, Y. Sun, D. W. K. Ng, and R. Schober, "Multiuser MISO UAV communications in uncertain environments with no-fly zones: robust trajectory and resource allocation design," *IEEE Transactions on Communications*, vol. 68, no. 5, pp. 3153–3172, 2020.

[16] H. Luo, Z. Liang, M. Zhu, X. Hu, and G. Wang, "Integrated optimization of unmanned aerial vehicle task allocation and path planning under steady wind," *PLoS One*, vol. 13, no. 3, article e0194690, 2018.

[17] M. Coombes, T. Fletcher, W. H. Chen, and C. Liu, "Decomposition-based mission planning for fixed-wing UAVs surveying in wind," *Journal of Field Robotics*, vol. 37, no. 3, pp. 440–465, 2020.

[18] F. Wang, J. Xu, X. Wang, and S. G. Cui, "Joint offloading and computing optimization in wireless powered mobile-edge computing systems," *IEEE Transactions on Wireless Communications*, vol. 17, no. 3, pp. 1784–1797, 2018.

[19] X. Zhang, Y. Zhong, P. Liu, F. Zhou, and Y. Wang, "Resource allocation for a UAV-enabled mobile-edge computing system: computation efficiency maximization," *IEEE Access*, vol. 7, pp. 113345–113354, 2019.

[20] H. Sun, F. Zhou, and R. Q. Hu, "Joint offloading and computation energy efficiency maximization in a mobile edge computing system," *IEEE Transactions on Vehicular Technology*, vol. 68, no. 3, pp. 3052–3056, 2019.

[21] M. A. Ullah, K. Mikhaylov, and H. Alves, "Enabling mMTC in remote areas: LoRaWAN and LEO satellite integration for offshore wind farm monitoring," *IEEE Transactions on Industrial Informatics*, vol. 18, no. 6, pp. 3744–3753, 2022.

[22] Y. C. Zhu and S. W. Wang, "Efficient aerial data collection with cooperative trajectory planning for large-scale wireless sensor networks," *IEEE Transactions on Communications*, vol. 70, no. 1, pp. 433–444, 2022.

[23] H. Zhao, G. Chen, H. Hong, and X. Zhu, "Remote structural health monitoring for industrial wind turbines using short-range Doppler radar," *IEEE Transactions on Instrumentation and Measurement*, vol. 70, pp. 1–9, 2021.

[24] L. D. Avendaño-Valencia, I. Abdallah, and E. Chatzi, "Virtual fatigue diagnostics of wake-affected wind turbine via Gaussian process regression," *Renewable Energy*, vol. 170, pp. 539–561, 2021.

[25] D. Xu, P. F. Liu, and Z. P. Chen, "Damage mode identification and singular signal detection of composite wind turbine blade using acoustic emission," *Composite Structures*, vol. 255, article 112954, 2021.

[26] K. Helsgaun, "General k-opt submoves for the Lin-Kernighan TSP heuristic," *Mathematical Programming Computation*, vol. 1, no. 2-3, pp. 119–163, 2009.

[27] A. G. H. Kek, R. L. Cheu, and C. Q. Meng, "Distance-constrained capacitated vehicle routing problems with flexible assignment of start and end depots," *Mathematical and Computer Modelling*, vol. 47, no. 1-2, pp. 140–152, 2008.

[28] K. Helsgaun, "An extension of the Lin-Kernighan-Helsgaun TSP Solver for Constrained Traveling Salesman and Vehicle Routing Problems," Dept People Technol, Roskilde Univ, Roskilde, Denmark, Tech Rep, 2017.

[29] R. T. Palomaki, N. T. Rose, V. D. M. Bossche, T. J. Sherman, and S. F. J. De Wekker, "Wind estimation in the lower

atmosphere using multirotor aircraft," *Journal of Atmospheric and Oceanic Technology*, vol. 34, no. 5, pp. 1183–1191, 2017.

[30] Y. Zeng, J. Xu, and R. Zhang, "Energy minimization for wireless communication with rotary-wing UAV," *IEEE Transactions on Wireless Communications*, vol. 18, no. 4, pp. 2329–2345, 2019.

[31] G. D. A. R. S. Bramwell and D. Balmford, *Bramwell's Helicopter Dynamics*, American Institute of Aeronautics & Astronautics (AIAA), Reston, VA, USA, 2nd edition, 2001.

[32] A. Filippone, *Flight Performance of Fixed and Rotary Wing Aircraft*, American Institute of Aeronautics & Astronautics (AIAA), Reston, VA, USA, 2006.

[33] W. Wang, W. P. Wang, and J. W. Wang, "Algorithm for finding the smallest circle containing all points in a given point set," *Journal of Software*, vol. 11, no. 9, pp. 1237–1240, 2000.

[34] Y. K. Son, S. Y. Lee, and S. K. Sul, "DC power system for fishing boat," in *Proceedings of the 2018 IEEE International Conference on Power Electronics, Drives and Energy Systems (PEDES)*, pp. 1–6, Chennai, India, 2018.